AUSTRALIAN JOURNAL OF CHEMISTRY

Preliminary investigation of a novel ^{18}F radiopharmaceutical for imaging CB2 receptors in a SOD mouse model

Journal:	*Australian Journal of Chemistry*
Manuscript ID	Draft
Manuscript Type:	Research paper
Date Submitted by the Author:	n/a
Complete List of Authors:	Pascali, Giancarlo; Prince of Wales Hospital Department of Nuclear Medicine and PET; University of New South Wales, School of Chemistry; Institute of Clinical Physiology National Research Council Panetta, Daniele; Institute of Clinical Physiology National Research Council De Simone, Mariarosaria; Institute of Clinical Physiology National Research Council Burchielli, Silvia; Fondazione Toscana Gabriele Monasterio per la Ricerca Medica e di Sanità Pubblica Lucchesi, Valentina; University of Pisa Sanguinetti, Elena; Institute of Clinical Physiology National Research Council Zanoni, Simone; University of New South Wales Iozzo, Patricia; Institute of Clinical Physiology National Research Council Saccomanni, Giuseppe; University of Pisa Manera, Clementina; University of Pisa Salvadori, Piero; Institute of Clinical Physiology National Research Council
Keyword:	Radiopharmaceuticals, Imaging agents, Fluorinated ligands, Receptors, Organic chemical synthesis

A Novel prospective CB2 tracer: radiosynthesis, early and late frames PET imaging in animal model.

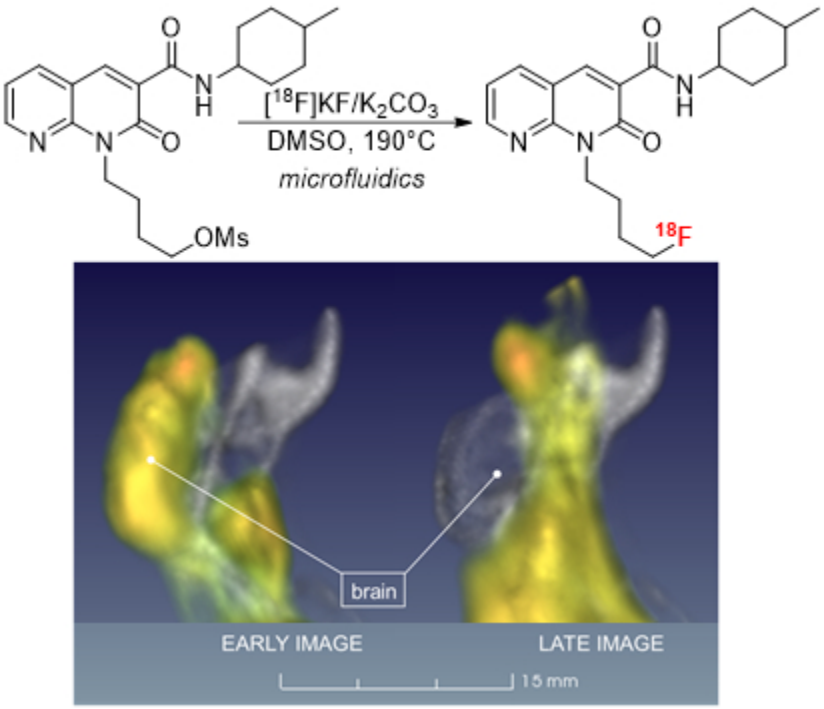
[18F]KF/K2CO3
DMSO, 190°C
microfluidics
OMs
18F
brain
EARLY IMAGE
LATE IMAGE
15 mm

Preliminary investigation of a novel ^{18}F radiopharmaceutical for imaging CB2 receptors in a SOD mouse model

Giancarlo Pascali[1,2,3], Daniele Panetta[3], Mariarosaria De Simone[3,4], Silvia Burchielli[3], Valentina Lucchesi[4], Elena Sanguinetti[3], Simone Zanoni[2], Patricia Iozzo[3], Giuseppe Saccomanni[4], Clementina Manera[4], Piero A. Salvadori[3].

Affiliations

[1] Nuclear Medicine Department, Prince of Wales Hospital, Barker Street, Randwick 2031, New South Wales, Australia

[2] School of Chemistry & Biological Resources Imaging Laboratory, University of New South Wales, High Street, Kensington 2052, New South Wales, Australia

[3] Institute of Clinical Physiology, National Research Council (CNR), Via G. Moruzzi, Pisa 56124, Italy

[4] Department of Pharmacy, University of Pisa, Via Bonanno Pisano, Pisa 56126, Italy

Abstract

We successfully radiolabelled a novel prospective cannabinoid type 2 receptor ligand with ^{18}F and tested its biodistribution in animal models by PET/CT imaging. The radiolabelling process was conducted on an alkyl mesylate fragment of the main naphthyridine core, using highly efficient microfluidic technology. No preliminary protection was needed, and the product was purified by semi-prep HPLC and SPE formulation, allowing to obtain the desired diastereomeric mixture in 29% RCY and >95% RCP. $SOD1^{G93A}$ mice were used as model of overexpression of CB2 receptors; PET imaging revealed a significant increase of the tracer distribution volume in the brain of symptomatic subjects compared to the asymptomatic ones.

Introduction

The cannabinoid (CB) receptor system is involved in numerous physiological processes and its functioning is mediated by two main subtype families, CB1 and CB2. Both receptor types are substrates for the same set of natural cannabinoid molecules, but they exert different effects, mostly linked to their tissue localization. In fact, while CB1 is mostly localized in the central nervous

system, thus modulating behaviour and feelings, CB2 is primarily expressed peripherally and involved in the inflammation cascade. For this reason, and due to their action, CB2 agonists have been assessed for their use as antinociceptives with reduced central effects. However, it has been reported that CB2 receptors are expressed in the brain during early neuroinflammatory processes, particularly in pre-activated microglia, and CB2 agonists have been tested for reducing neuronal degeneration and improving cognitive functional scores.[1] Therefore, due to the low natural abundance of CB2 in the healthy brain, it has been suggested to use selective CB2 tracers to identify the neuroinflammation phenomena that are linked to several neurodegenerative diseases, such as Parkinson's (PD), Alzheimer's disease (AD), Amyotrophic Lateral Sclerosis (ALS), in order to provide a specific tool for diagnosis and therapeutic follow-up.

Following this lead, we initiated a research program aimed at designing and testing novel Positron Emission Tomography (PET) radiopharmaceuticals for imaging the CB2 receptor population in genetically modified animal models mimicking ALS.

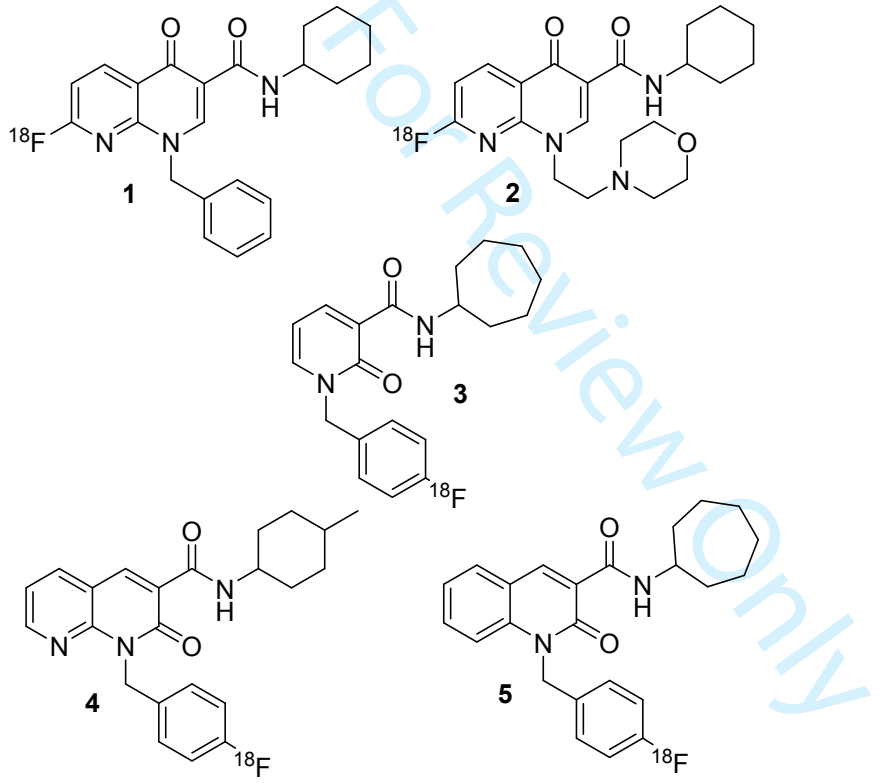

Figure 1: CB2 radiopharmaceuticals previously reported by our group, based on the naphthyridine, quinoline and pyridine scaffold.

We have recently described the synthesis and pharmacological properties of a series of 1,8-naphthyridin-2(1H)-one-3-carboxamides with high potency and selectivity for CB2 receptors.[2–5] Our initial studies[6] on radiofluorinating these scaffolds revealed the instability of the carbon-fluorine bond, as we noticed extensive defluorination in *ortho* position of the pyridine-like nitrogen of **1** and **2**.[7,8] In successive studies, we have investigated structures **3**, **4** and **5**, bearing a more stable fluorobenzyl moiety,[9] but the synthesis of the radiolabelling precursor, as well as the radiofluorination process itself, resulted to be quite challenging (Figure 1). We have therefore directed our attention to structures bearing a fluoroalkyl moiety, forecasting easier radiochemical access and good stability.

Table 1: Pharmacological properties of investigated CB2 ligands.

Compound	Ki CB2 (nM)	Ki(CB1)/Ki(CB2)	LogP
1	51.8	9.6	3.83
2	370	>27	1.94
3	7.9	5	3.04
4	0.9	222	3.53
5	0.24	48	4.16
11	1.36	743	2.39

Among the candidates of the molecular lead developed, compound **11** showed good potency and CB2 selectivity, LogP in the 1-3 range and reliable synthesis (Figure 2).[3] In particular, the synthetic route adopted involved the production of the mesylate intermediate **10**, that represents a suitable radiofluorination precursor. In this work we will describe the production of **[^{18}F]11** and its biodistribution in an ALS mouse model, based on a genetically modified superoxide dismutase 1 (SOD1).

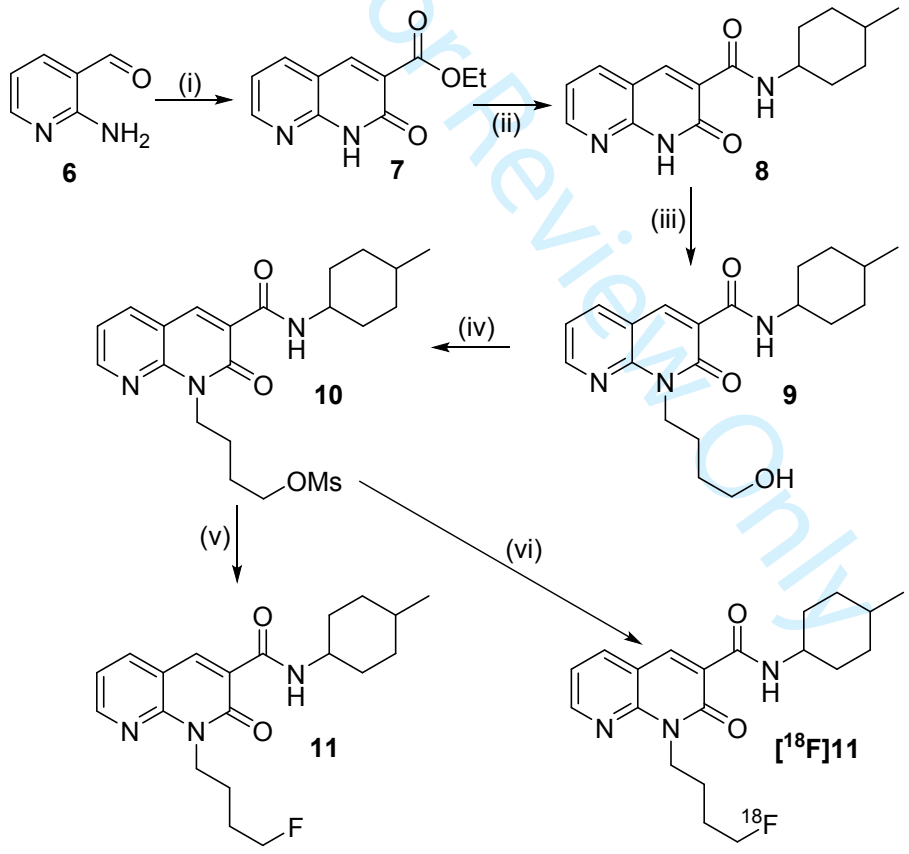

*Figure 2: Synthetic route for **11** and **[^{18}F]11**. (i) Diethyl malonate, piperidine, EtOH, reflux, 24h; (ii) 4-methylcylohexylamine, MW, 140°C, 1h 200W; (iii) NaH, DMF, chlorobutanol, 50°C, 24h; (iv) triethylamine, methanesulfonyl chloride, dichloromethane, 0-25°C, 6h; (v) Tetrabutylammonium fluoride, THF, reflux, 4h; (vi) [^{18}F]KF, K_{222}/K_2CO_3, DMSO, microfluidics, 190°C.*

Results and discussion

Radiolabelling optimization

The radiofluorination of **10** was performed using an Advion NanoTek microfluidic system. The use of this apparatus allowed to streamline the optimization of reaction conditions while minimizing chemicals, radioactivity and time employed.[10] The ^{18}F complex was prepared as previously described[6] using DMSO as reconstituting solvent, and it was loaded in the storage loop of Pump3, while the mesylate precursor was dissolved in DMSO (11.8 mg/mL) and loaded in the storage loop of Pump1; a 15.6 µL flow microreactor was used for all the experiments. In these experimental set, the starting activity was 5.8 GBq, and 15-20 µL of fluorinating complex was used in each bolus reaction, bearing an activity ranging from 120 to 40 MBq (due to decay in the 2.5 hours of the optimization process). Reaction parameters were varied in the process as follows: reaction temperature (110-190 °C), reactants residence time (9.4-93.8 sec), mass of precursor (178.5-2380 µg). The crude reaction mixtures were analysed by both Radio-HPLC and Radio-TLC, reporting equivalent trends but a slightly higher radiochemical yield (RCY) by TLC.

Graphs from these experiments are shown in Figure 3. From these results, it was possible to identify that temperature had the main effect on RCY, which increased at higher T, and reached its highest value at 190°C. Residence times did not provide a clear trend at 190°C, while at 170°C it seemed that using lower flow rates (i.e. longer residence time) provided higher RCY. Precursor mass contribution used in each bolus reaction was tested at 170°C and did not provide significant variation in RCY, except a noticeable decrease at the lowest value of 178.5 µg.

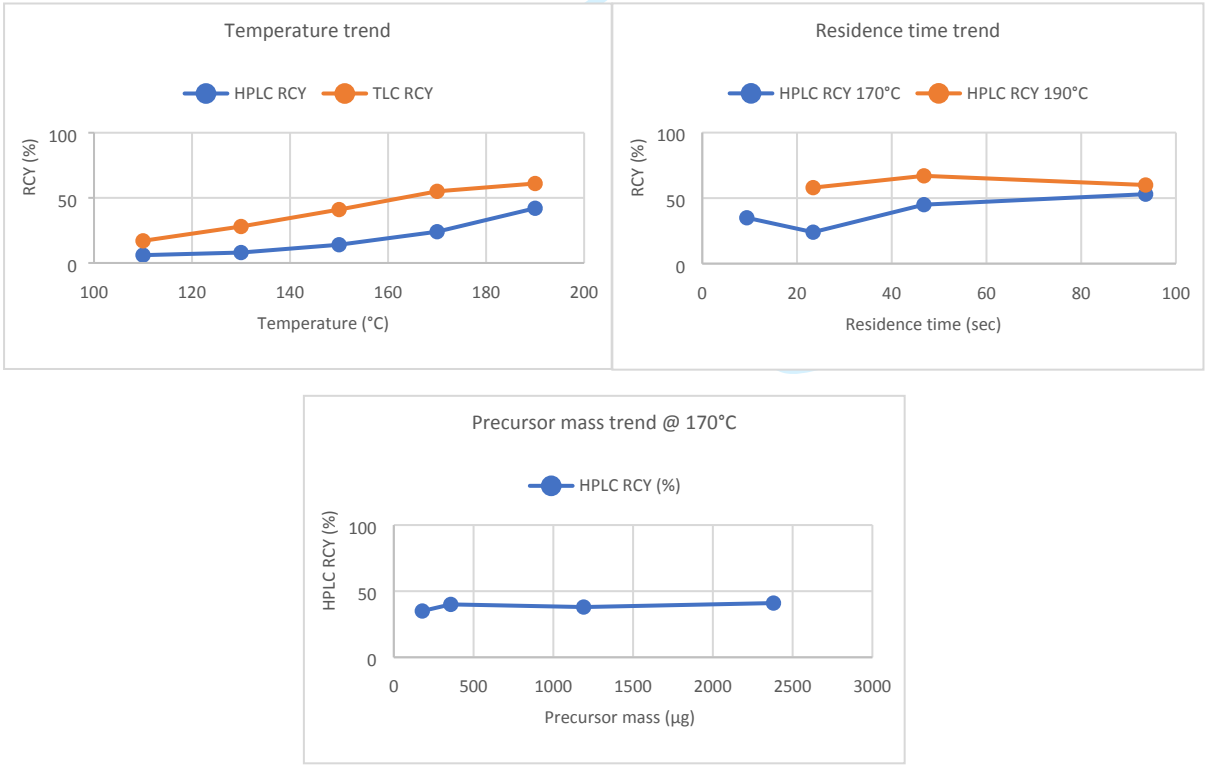

*Figure 3: Trend graphs for radiofluorination of **11** with modification of T, residence time and precursor mass.*

Production of [^{18}F]11

The advantage of using a microfluidic system for both optimization and production is due to the capability to directly scale up the process without needing to re-optimize for higher activities.[11,12] In order to meet an optimal trade-off for process length and high yield, it was decided to use a temperature of 190°C and a residence time of 23.4 sec, given by a 1:1 ratio of 20 µL/min flow for each channel (radiofluorination and precursor solutions). Since higher amount of activity are needed for preclinical preparation runs, higher starting activity and a maximum volume of 200 µL for both solutions was used; this allowed to reduce the concentration of the precursor to 1.2-1.3 mg/mL that, when used in the production radiolabelling run, would provide a total bolus reaction mass of 240-260 µg. Using larger bolus volumes was also expected to provide higher RCY, given the positive bolus-effect reported for this microfluidic approach.[13]

The hardware utilized in the production was modified as previously described[14] to allow reaction, purification and formulation to be controlled by the same software. More in detail, the output of the flow system was directed towards the storage loop of a manual HPLC injector, connected to an external pump and semi-prep column. The outlet of the chromatographic column was monitored by a customized radioactivity probe[15]; this allowed to detect the product fraction, that was directed to a separate vial for water dilution. This diluted fraction was then passed through a C-18 SPE cartridge, that retained the organic product. The SPE was eluted with EtOH and the ethanolic fraction evaporated and reconstituted with a 10% ethanolic injectable saline. This production process was used in 16 runs, of which 4 had issues mostly related to loss of activity in the initial phases of the production (radioactive fluoride pre-concentration, drying and reconstitution). Effectively, no failures were recorded from the flow radiolabelling onwards.

Schema 9

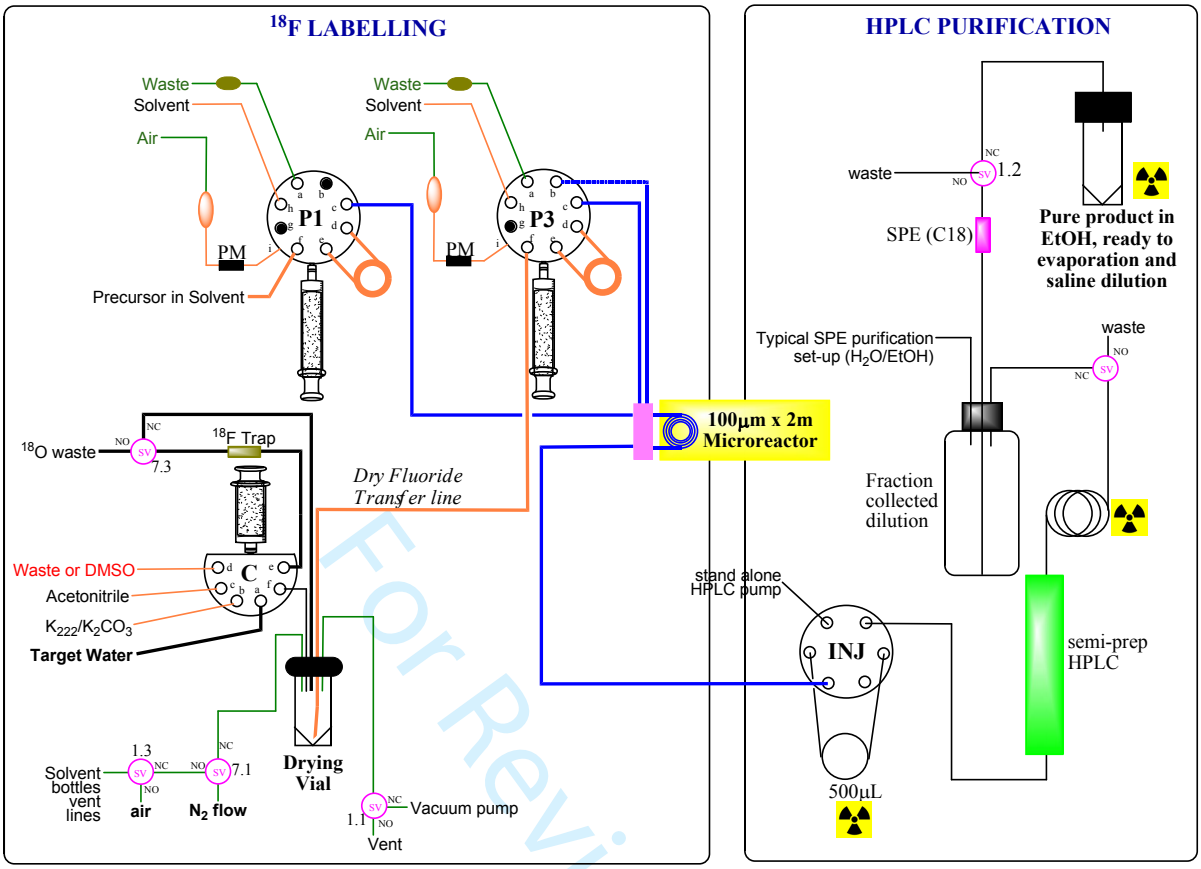

*Figure 4: Schematic of the synthetic apparatus used for the production of [^{18}F]**11**.*

The semi-prep chromatographic separation highlighted a peculiar point, linked to the diastereoisomerism of **11**. In fact, in the typical purification run, two radioactive peaks of similar heights were detected, and they were due to the presence of *cis* and *trans* conformers at the methylcyclohexyl substituent. In fact, also the precursor **10** was used as diastereoisomeric mixture and no attempt was done on purifying this precursor or synthesize the diastereoisomerically pure compound, as the biological assay for **11** was tested with such mixture.

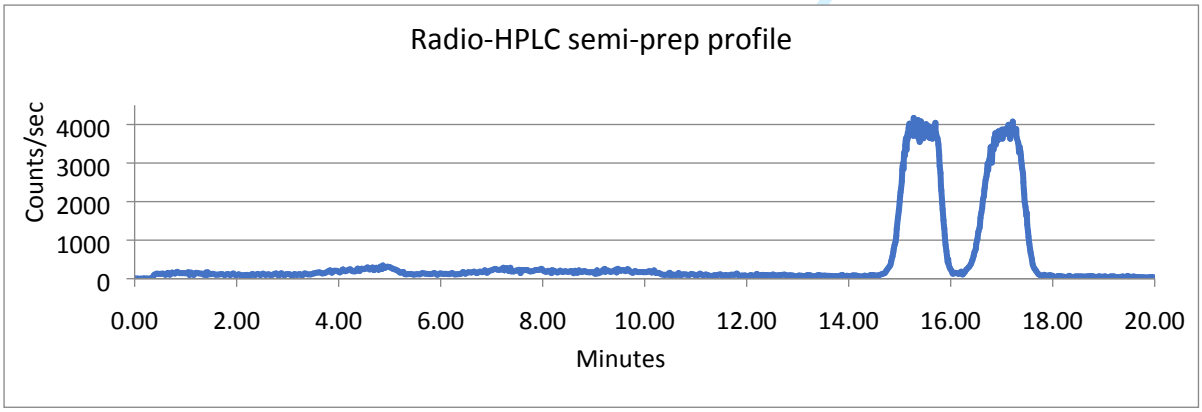

*Figure 5: Typical radioactive chromatographic profile for the purification of [^{18}F]**11**.*

In the preclinical production runs, a starting activity of 34.4±6 GBq was used, and such radiofluoride solution was pre-concentrated, dried and reconstituted as previously reported;[6] for this process, 0.7mL of DMSO were used as reconstituting solvent, to provide the radiofluorinating mixture. In a

typical run, 200µL of this mixture was processed as described, yielding 845±393 MBq of **[^{18}F]11**, that was >95% radiochemically pure and with a molar activity (A_M) of 25±14 MBq/nmol at end of synthesis (EOS).

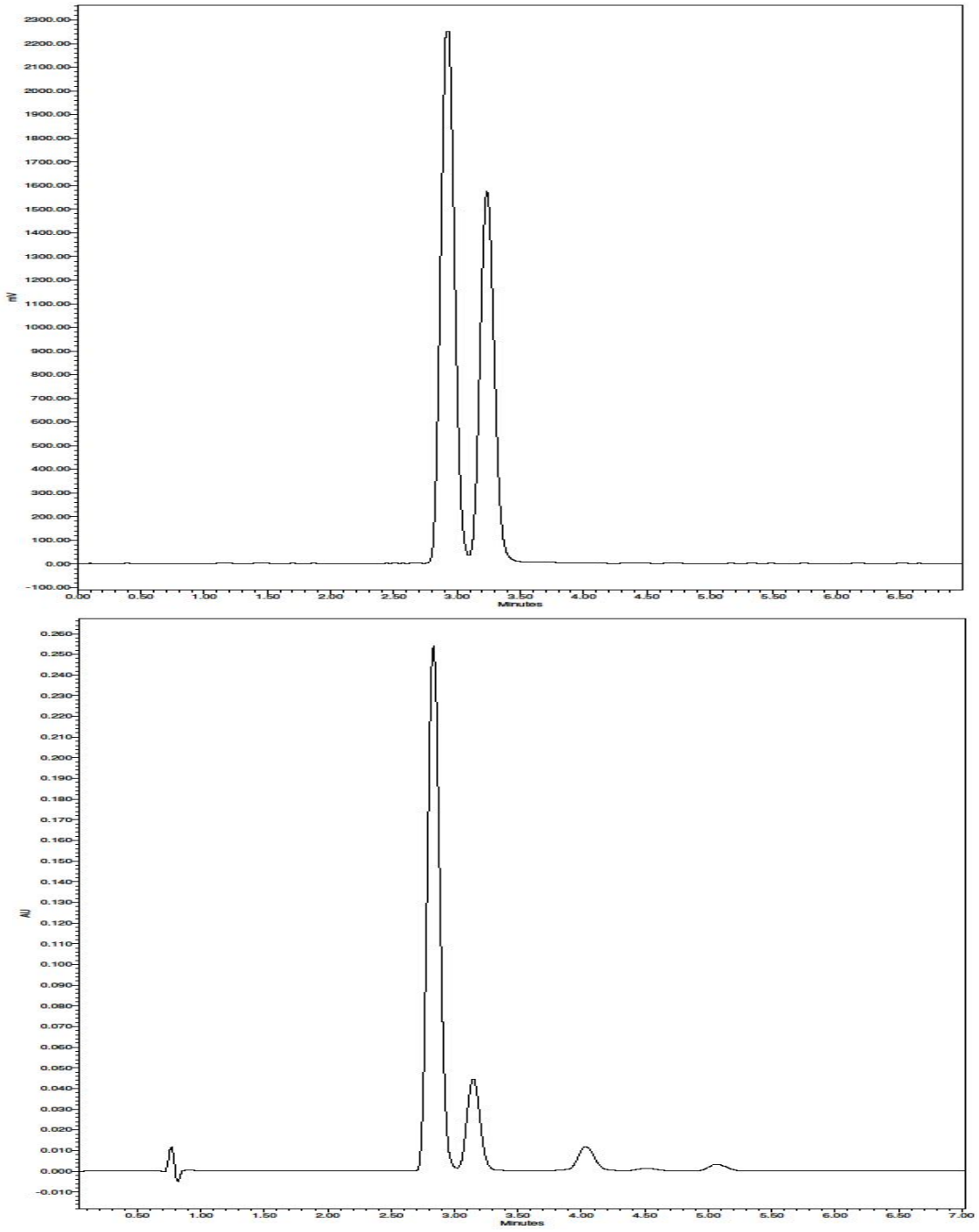

Figure 6: Representative HPLC analysis of final product. Top: radioactivity trace; bottom: UV trace at 344nm

The overall process was divided into two phases, namely a) radiofluorinating mixture preparation and b) tracer production. On average, phase a) lasted 40 min, while phase b) lasted 50 min; however, due to concurrent animal and scanner preparation, phase b) was not always started right after phase a). This feature, added to the reported variability in recovering the radiofluorinating mixture,[16] made difficult to evaluate the RCY of the process. In this case, we evaluated this parameter by performing a sample radiofluorination reaction at EOS and measuring it for

radioactivity content. By this method, we estimated a RCY of 29±12%, that is lower than the unpurified RCY, but still allowed to scan up to 3 subjects per production run during imaging sessions.

Animal models

In this work we were interested in evaluating the differential uptake of **[^{18}F]11** in an animal model featuring ALS. Mutations in the antioxidant enzyme Cu/Zn superoxide dismutase 1 (SOD1) gene have been linked to the cause of approximately 20% of familial ALS. Expression of a mutant human SOD1 transgene in mice (i.e. SOD1^{G93A} mice) results in altered motor neuron functioning, thus inducing symptoms mimicking human ALS, making this model the most widely used for studies on this disease.[17] Neuron degeneration and death is accompanied by microglia activation, which represents a hallmark of neuroinflammation. In particular, microglia priming, i.e. before phagocytosis is exerted, is associated with an up-regulation of CB2 receptors,[18] and this is also readily apparent in SOD1^{G93A} mice;[19] therefore, we forecasted this to be a good model to evaluate the imaging profile of **[^{18}F]11**.

SOD1^{G93A} mice develop evident symptoms at 12-16 weeks, represented by progressive motor deficits (tremor and shaking in one or more limbs) leading to paralysis.[20] In our study, we have monitored the mice for occurrence of locomotor symptoms, and scanned both asymptomatic (n=11) and symptomatic (n=11) SOD1^{G93A} to assess the potential diagnostic value of CB2 imaging. We also studied **[^{18}F]11** in CD1 (n=3) and C57BL (n=4) mouse strains, as reference models for healthy subjects. In addition, blocking experiments with commercially available CB2 receptor agonist (AM630) have been performed on 5 SOD1^{G93A} animals, 3 of which were clearly symptomatic, while the others (121 days old) were studied just before symptoms onset.

Quantitative autoradiography (QAR)

In order to assess the binding of **[^{18}F]11** in the tissues of interest, we performed in vitro autoradiography assay using brain slices obtained from CD1, SOD1 mice, which included primary motor cortex (MC) and cerebellum (C). The slices were incubated with a solution of **[^{18}F]11** and then exposed onto a phosphor plate for radioactive imaging. Pre-blocking studies were also conducted by incubating contiguous slices with the CB2 ligand AM630 prior to radiopharmaceutical incubation, to assess the level of specificity of **[^{18}F]11** for the target.

Radioactive distribution was obtained by laser scan of the phosphor plates, recorded in digital light units (DLU) and corrected for regions of interest (ROI) area; ROI in the slices were identified and drawn manually. Specificity of **[^{18}F]11** uptake was calculated as:

$$Spec(\%) = \frac{(Act_0 - Act_b)}{Act_0} \times 100$$

Where Act_0 and Act_b are the DLU/mm^2 values for unblocked and blocked slices. Applying the calculation, we obtained an average specificity in the MC tissue of 31±15% for CD1 and 21±10% for SOD1 animals. Peculiarly, the SOD1 animals showed a distinctive asymmetry in uptake, that revealed a repeatable higher specific uptake in the right emisphere *vs* the controlateral (24±12% *vs* 17±11%). In the cerebellum, a negative specificity of -13.3 ±10.3% was determined.

From this data, it is possible to assume that **[^{18}F]11** shows a reasonable specificity in the brain and, in particular, in MC areas, that could be indeed involved in the movement disorders observed in SOD1 subjects; likewise, the observed left-right difference might be related to the asymmetric appearance of movement disorders, although we cannot make any inference on this point as symptoms were not recorded following this parameter during animal monitoring.

PET/CT imaging

PET and CT imaging of all animals were carried out by using a YAP-(S)PET II microPET and a XALT high resolution scanner, respectively, as explained in the Methods section.

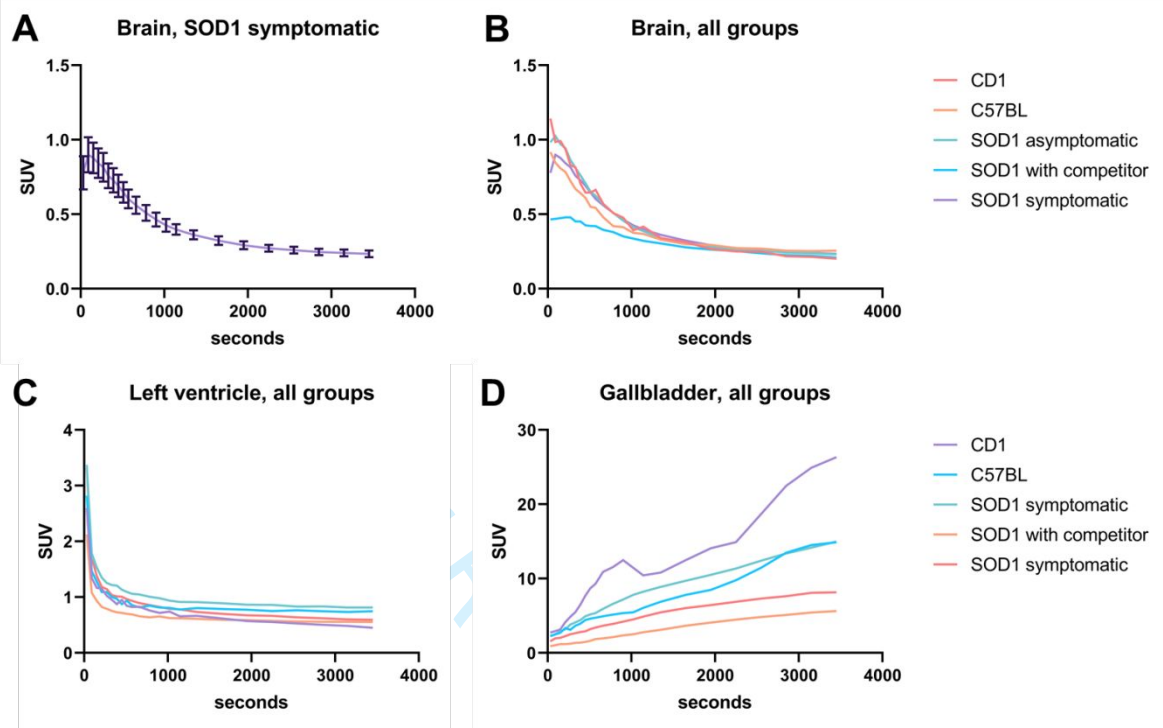

Figure 7: TAC for the WB region in the SOD1 symptomatic population, reporting average and error as %SEM (A); TAC for WB region for all the study groups, reporting as average (B); TAC for the LV region for all the study groups, reported as average (C); TAC for the GB region for all the study groups, reported as average (D).

ROI were manually drawn on three organs: cardiac left ventricular cavity (LV), whole brain (WB) and gallbladder (GB). The LV was used to evaluate blood compartment and the related input function, WB represented the target organ, while GB showed a peculiar high accumulation, possibly related to excretion. Time Activity Curves (TAC) were evaluated from the raw Bq/mL data, corrected for injected dose and animal weight; examples of TAC are reported in Figure 7.

The data obtained from the different groups showed considerable variability (Figure 7A) that did not allow to reach a significantly low p value in any group comparison. Average values for each time-point in each group revealed a delayed washout from the WB region (Figure 7B) when compared with LV TACs (Figure 7C). Gallbladder accumulation of CB2 radiolabelled tracers has been reported in previous studies,[21] and we have noticed this phenomenon also in our experiments (Figure 7D).

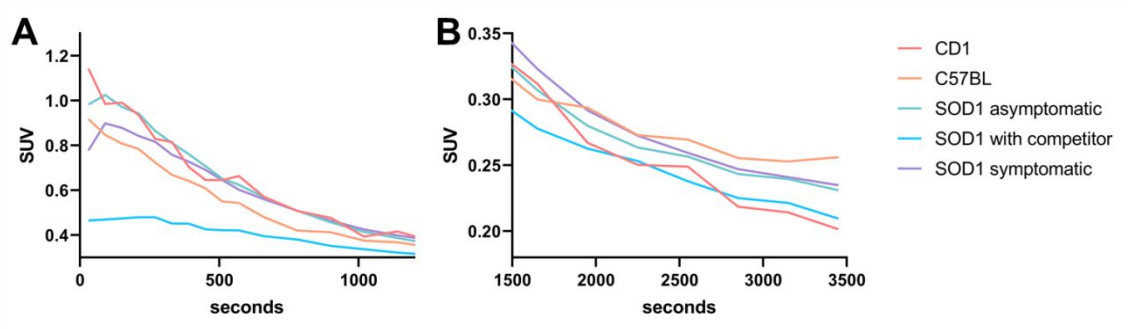

Figure 8: Whole brain (WB) TAC for all study groups, early (A) and late frames (B).

A comparison between early and late frames of the WB TACs showed trend differences between study groups. While in the first 5 minutes CD1 and C57BL groups (i.e. control subjects) showed an immediate decline washout, in both unblocked groups of SOD1 mice we observed a noticeable uptake; on the other hand, the SOD1 group receiving a pre-blocking dose of competitor was characterized by markedly lower SUV values in these same early frames (Figure 8A). This differential uptake among groups, in particular with the competitor population, disappeared in the later time points (Figure 8B), showing a clear washout from WB region (Figure 9). This finding suggests the redistribution of the competitor over time due to reversible CB2 receptor binding of the tracer.

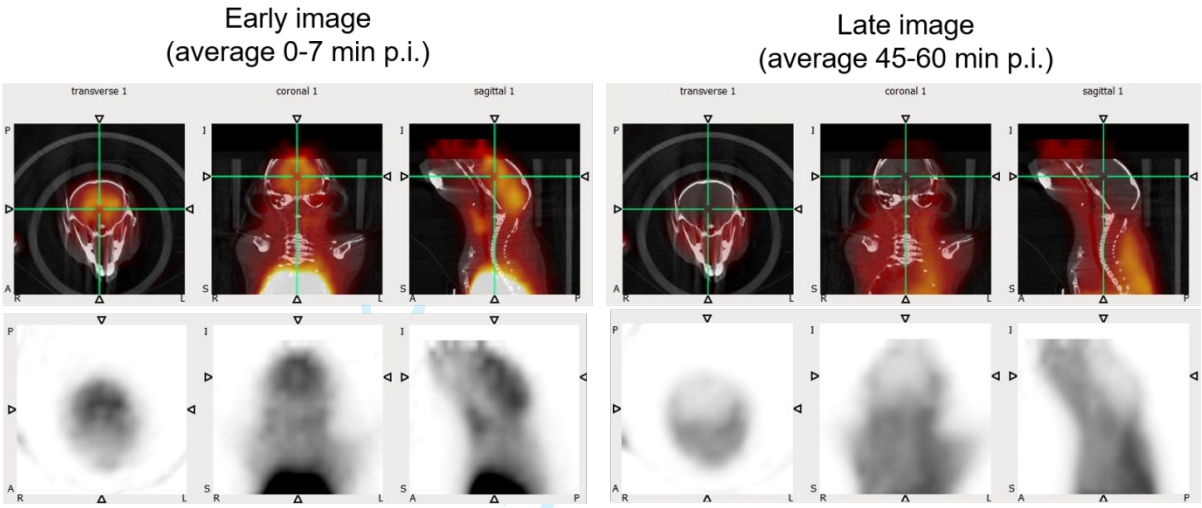

Figure 9: PET images example for SOD1 mouse (asymptomatic), centred on the WB region. Left: first 7 min frames averaged; right: last 5 min frames averaged

Therefore, we analysed the data using a Logan plot to assess group differences in tissue Distribution Volume Ratio (DVR).

Logan analysis of dynamic uptake

Logan plot is a graphical method for the quantification of PET imaging data developed for reversibly binding radiotracers with rapid dissociation constants and efflux from tissue. Moreover, this method concerns tracers whose kinetic can be described in terms of first-order, constant-coefficient, linear differential equations. In its original version, the arterial plasma tracer concentration represents the input function.[22] However, when a non-receptor-containing region is present, like in this study, blood sampling can be avoided, and the Logan method can be adapted to use that region as reference.[23] In our case, we used the LV data as reference to estimate DVR, which is defined as:

$$DVR = \frac{DV_{tissue}}{DV_{ref}} = BP + 1 \quad (1)$$

where DV_{tissue} and DV_{ref} are the distribution volume in the target tissue and in the reference one, and BP is the binding potential.[24] Following this definition, higher values of DVR reflect an increased expression of the target in the tissue of interest. In the Logan plot, a linear trend is reached after a certain time (t > t*), in which the slope represents the DVR, according to:

$$\frac{\int_0^t C_{tissue}(\tau)d\tau}{C_{tissue}(t)} = DVR\frac{\int_0^t C_{ref}(\tau)d\tau}{C_{tissue}(t)} + q \quad (2)$$

where $C_{ref}(t)$ and $C_{tissue}(t)$ are the tracer concentration in the reference tissue (LV) and in the target tissue (WB), respectively. The term including the average tissue-to-plasma efflux constant (q) was omitted because the ratio of $C_{tissue}(t)$ over $C_{ref}(t)$ is assumed to be reasonably constant.[23]

The optimal value of t* was chosen by visual inspection of all the Logan plots and set to use at t = x min (i.e. the last 7 time points). The selection of earlier or later time points (namely 5 to 10) yielded consistent results with average percentage difference of DVRs less than 4%.

Finally, the least square estimation of DVR was weighted using the inverse of the variance of the PET measurement, calculated as:[25]

$$var(t_k) = \frac{C(t_k)}{\Delta t_k} \tag{3}$$

where $C(t_k)$ is the acquired mean value of the tracer activity over the k^{th} relative time scan interval Δt_k.

The Logan analysis was implemented in MATLAB R2020a (The MathWorks, Natick, MA, USA), using the *cumtrapz.m* function to perform the cumulative trapezoidal numerical integrations shown in equation (2).

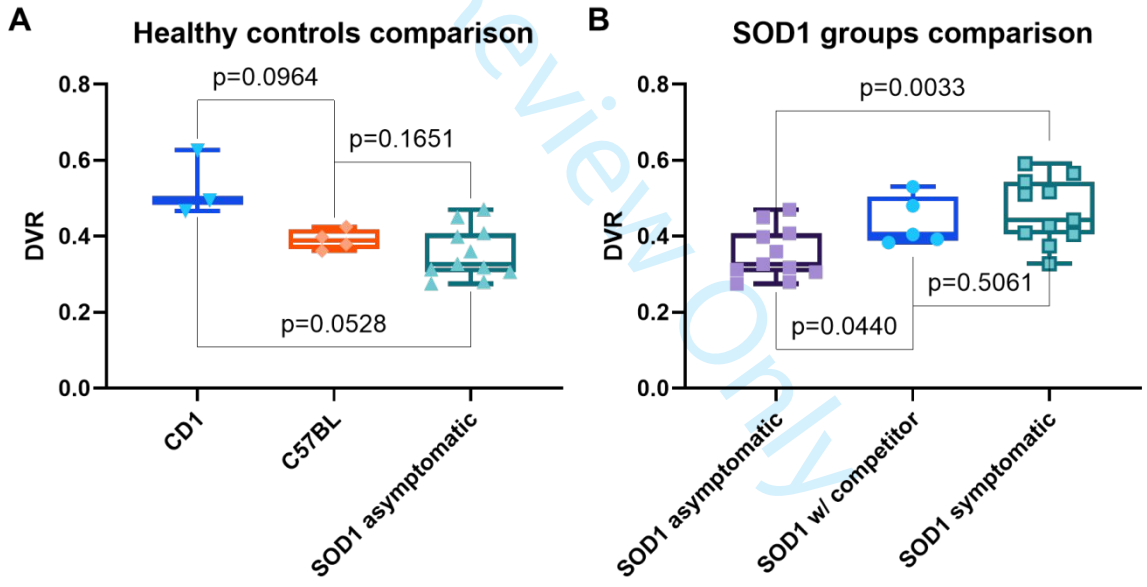

Figure 10: Box plots of DVR values, comparing control groups and SOD1 asymptomatic (A) and all SOD1 groups (B).

DVR findings were compared to assess binding differences in the target tissue between groups, assuming a p value <0.05 as significant; in particular the higher the DVR, the higher the binding in the target tissue. The DVR was similar between the healthy groups, CD1 and C57BL, and the asymptomatic SOD1 mice. However, the C57BL group featured a higher similarity with the transgenic group (p=0.1651, Figure 10A), whereas the difference seems more pronounced with the CD1 group (p=0.0528), in which significance was almost achieved. Interestingly, the $SOD1^{G93A}$ mice have a (C57BL/6 x SJL)F1 strain of origin,[26] and this finding may points out the importance of preferring the C57BL strain as control model.

A significant difference in DVRs was instead found between asymptomatic and symptomatic SOD1 groups, (p=0.0033) (Figure 10B). This finding strongly supports that an increased expression of CB2 receptors occurs during disease progression in this animal model.

The DVR from the group in which a competitor was used was significantly different from the asymptomatic SOD1 group (p=0.0440) and equivalent to the untreated symptomatic group (p=0.5061); a potential explanation is that the competition test was performed on overtly symptomatic (n=3) or late asymptomatic (n=2) subjects, which were age matched, thus potentially already presenting the biochemical hallmark of disease progression.

Conclusion

This work describes the radiolabelling and the preliminary *in vivo* biodistribution of a prospective PET radiopharmaceutical for imaging the CB2 receptor, based on a naphthyridine core and labelled with ^{18}F on a side alkyl chain bearing a mesylate group. The radiolabelling process, as performed via microfluidics, semi-prep HPLC purification and SPE formulation, allowed to obtain the desired product in 29% RCY with a A_M=24 MBq/nmol EOS. *In vitro* autoradiography and competition tests were also used to preliminarily explore radiotracer specificity in the brain and cerebellum. The biodistribution of the radiolabelled product was studied using PET/CT imaging in Superoxide Dismutase 1 gene model mice (SOD1^{G93A}), and in CD1 and C57BL mice as healthy controls. SOD1 mice were divided into asymptomatic and symptomatic groups. Our investigation was focused on assessing the radioactive uptake in the brain regions. A Logan plot analysis was conducted to estimate differences in the Distribution Volume Ratio (DVR) in the brain between healthy, asymptomatic and symptomatic SOD1 groups as a possible indicator of early specific extraction of the tracer in a highly reversible mode. This analysis revealed a significant difference between asymptomatic and symptomatic SOD1 animals, where the symptomatic SOD1 had a markedly higher DVR. Such outcome is in line with the research hypothesis that an increased CB2 receptor expression occurs in the symptomatic subjects, and may support the potential use of **[^{18}F]11** as PET imaging tracer for CB2 receptors in the brain. Further studies would be required to fully understand the whole-body distribution of such molecule, its metabolism and the inter-species uptake differences.

Experimental

Radiochemistry

General: All chemicals and solvents were purchased from Sigma-Aldrich and used without further purification. The high-purity grade solvents were vented through a soda lime/molecular sieves trap upon use. Micro-SPE cartridges MP-1 were purchased from ORTG (USA). [^{18}F]fluoride was produced at a PETtrace cyclotron (GE Healthcare, USA) by proton bombardment (Ep= 16.7 MeV, 5-15 min at 20-25 µA) of a 1.3 mL [^{18}O]water (enrichment > 98%) silver target. Preparative Radio-HPLC were run using isocratic conditions (60/40=CH_3CN/H_2O at 3mL/min) using a standalone Waters 515 pump, a Rheodyne 7125 manual injector, a Phenomenex Synergi Fusion-RP 80A (4µm, 250x10mm) column, while radioactive peaks were monitored by a prototype CsI scintillator detector (Tyndall, Ireland).[15] Analytical Radio-HPLCs were obtained using a Delta 600 pump system (Waters, USA) equipped with a Gabi Star flow-through gamma detector (Raytest, Germany) connected in series to a 996 Photo Diode Array (PDA) UV detector (Waters, USA) on a Phenomenex Synergi Hydro-RP 80A (4µm, 150x4,6mm) using 65/35=CH_3CN/H_2O. TLC analyses were performed using silica plates and 100% EtOAc as eluent and acquired using a Cyclone PLUS (Perkin-Elmer, USA).

Radiosynthesis was performed using an Advion microfluidic system equipped with a 15.6 µL internal volume microreactor. The apparatus has been customized for performing automatically HPLC peak collection and SPE formulation of the collected peak.[14]

Production of **[^{18}F]11**: A 1.2±1 mg/mL solution of **10** in dry DMSO was prepared from ten-fold concentrated stock solution; this precursor was charged into the storage loop of Pump 1 (P1). The dry fluorination complex was prepared as previously reported,[6] employing 15±1 mg/mL of K_{222} in CH_3CN and 80µL of a 50 mg/mL solution of K_2CO_3 in H_2O. The dried residue was reconstituted with 0.7 mL of DMSO and this solution was charged into the storage loop of Pump 3 (P3). In order to prime the flow system, three "dummy" reactions were performed by delivering into the microreactor 30, 10 and 10 µL at 20µL/min for each channel at respectively 150, 170 and 190°C. The actual production was performed by delivering 200µL from P1 and P3 at 20µL/min into the microreactor heated at 190°C; the reaction mixture was directed towards the 0.5mL loop of a manual injector valve. The isocratic elution conditions used allowed to collect the radioactive product as a double peak (two conformers) at approximately 15 and 17 min.

The collected fractions were diluted with water, passed on a C18 Waters Sep-Pak C18 Plus Light and the product was eluted with 1.5mL of EtOH. The obtained ethanolic solution was dried and the residue reconstituted with a suitable volume (0.5-2mL) of 10% ethanolic saline and sterile filtered. The product was ready for animal injection (518-1380 MBq) with an estimated RCY of 29±12% (from the starting fluoride complex solution). The whole production process took around 50 min from the start of bolus delivering to obtaining the injectable solution. The product was >95% radiochemically pure by both HPLC and TLC and A_M was 25±14 MBq/nmol at EOS.

Quantitative autoradiography

Animals were housed in light and temperature controlled conditions (12 hrs light:12 hrs dark; 22±2°C) and given ad libitum water and food. All procedures were performed using protocols approved by the Institutional Animal Care and Use Committee. At sacrifice, all mice were deeply anesthetized and brains were promptly removed, washed in PBS 1X (pH=7,4) and then individually included in OCT matrix. After freezing with dry ice, samples were stored at -80°C until sectioning in 20 µm-thick coronal sections by cryostat.

The obtained tissue sections of primary motor cortex, red nucleus-midbrain and cerebellum were collected and placed on poly-lysine-coated glasses slides. Each area was studied in duplicate. Tissue sections were heat-fixed for 5 min at 50°C with an heating chamber and then pre-blocked or not with 100 µL of antagonist saline solution (AM630, 15 µM) for 45 min. Pre-blocker sections were washed three times with phosphate buffer 1X (pH=7,0) before incubation. Brain tissue slices were incubated for 1 h with 100 µL of **[^{18}F]11** (0,8 MBq/mL). During the incubation time at room temperature, the tissue sections were placed in a humidified black box to reduce evaporation. The excess of radioactivity was washed thrice by phosphate buffer 1X. The sections were then dried and exposed to phosphor plate for 1 min, before being scanned using a Cyclone Plus. The intensity of *ex vivo* auto-radiographic images was measured using Optiquant software (Perkin Elmer, USA) by manually drawing ROI, and the raw data were evaluated using Microsoft Excel.

Study populations

A total of n= 34 mice (The Jackson Laboratories, Bar Harbor, Maine) were employed for the study. Specifically, we studied 3 animals groups: CD1 (n=3), C57BL (n=4) and SOD1^{G93A} (n=27). Within the SOD1 group, mice were classified as follow: n=11 as asymptomatic (age=72-114 days), n=11 as symptomatic (age=137-175), and n=5 employed in pre-blocking experiments with AM630. All mice

were housed under 12-hour light/12-hour dark cycles and controlled room temperature (22 °C), with *ad libitum* access to food and fresh water. Health status and locomotor abilities were regularly monitored, and underwent PET/CT imaging as required: abnormally reduced activity, hindlimb suspension, beam walk, limb tremor o shaking were used to classify SOD1 mice as symptomatic. At the end of *in vivo* procedures, all animals were euthanized. The experimental protocol was conducted in accordance with the D.L.116/92 implementation of European Economic Community directive 609/86 regarding the protection of animals used for experimental and other scientific purposes.

PET/CT imaging protocol and analysis

Prior to imaging, anaesthesia was induced by xylazine and ketamine and maintained by gas inhalation of isoflurane. The tail veins were accessed and catheterized for tracer administration. CT imaging was performed for anatomical co-localization of PET images using the XALT scanner,[27] with animals in supine position, with the following settings: 35 kV, 1 mm Al filtration, 211 views over 200° (short-scan), 0.27 mAs/view, 80 s total scan time. Images were reconstructed with custom cone-beam FBP algorithm on 3D matrices of 480x480x720 voxels, with an isotropic voxel size of 84 micron. Upon completion of the CT scan, animals were transferred on the same carbon fiber bed to the PET scanner (YAP(S)PET II, I.S.E. s.r.l., Vecchiano, Italy). Animals received an i.v. injection of 3-17 MBq (median: 7.7 MBq) of tracer depending on their weight in 100-200 μl dilution volume, followed by 100 μl of saline. A 60 min dynamic PET scan of the brain region was performed immediately after injection. PET images were reconstructed using an iterative OSEM algorithm, as previously described,[28,29] on a 3D matrix size of 128x128x27 slices (voxel size: 0.375x0.375x1.5 mm3). The dynamic protocol was set up with the following time frames: 9x 60s; 5x 120s; 8x 300s. After the dynamic scan, a whole-body multi-bed position static PET scan was performed, with the total duration of 15 min (5 min per bed position). All images were corrected for random coincidences, dead time, decay correction, and calibrated in kBq/cc. ROI drawing was performed on Amide software (http://amide.sourceforge.net/), using a cylindrical volume for LV (1.5x1.5x3 mm, drawn from first 2 frames), an ellipsoid for WB (4x7x3 mm, drawn from last 2 frames) and an ellipsoid for GB (2x3x2 mm, drawn from last 2 frames). Time activity curves (TAC) were then derived on each animal, and standardised uptake value (SUV) curves were calculated by correcting for injected dose and animal weight.

Acknowledgements

We thank the Australian National Imaging Facility for support. These results were obtained within the project Positron Emission Tomography and Lateral Amyotrophic Sclerosis (PETALS II) funded by the Fondazione Italiana di Ricerca per la Sclerosi Laterale Amiotrofica (ARISLA). The authors declare no conflict of interests.

References

[1] S. Yamagishi, Y. Iga, M. Nakamura, C. Takizawa, D. Fukumoto, T. Kakiuchi, S. Nishiyama, H. Ohba, H. Tsukada, K. Sato, Y. Ouchi, *J. Neuroinflammation* **2019**, *16*, 208.

[2] C. Manera, G. Saccomanni, B. Adinolfi, V. Benetti, A. Ligresti, M. G. Cascio, T. Tuccinardi, V. Lucchesi, A. Martinelli, P. Nieri, E. Masini, V. Di Marzo, P. L. Ferrarini, *J. Med. Chem.* **2009**, *52*, 3644–3651.

[3] V. Lucchesi, D. P. Hurst, D. M. Shore, S. Bertini, B. M. Ehrmann, M. Allarà, L. Lawrence, A. Ligresti, F. Minutolo, G. Saccomanni, H. Sharir, M. Macchia, V. Di Marzo, M. E. Abood, P. H. Reggio, C. Manera, *J. Med. Chem.* **2014**, *57*, 8777–91.

[4] C. Manera, V. Benetti, M. P. Castelli, T. Cavallini, S. Lazzarotti, F. Pibiri, G. Saccomanni, T. Tuccinardi, A. Vannacci, A. Martinelli, P. L. Ferrarini, *J. Med. Chem.* **2006**, *49*, 5947–5957.

[5] C. Manera, G. Saccomanni, A. M. Malfitano, S. Bertini, F. Castelli, C. Laezza, A. Ligresti, V. Lucchesi, T. Tuccinardi, F. Rizzolio, M. Bifulco, V. Di Marzo, A. Giordano, M. MacChia, A. Martinelli, *Eur. J. Med. Chem.* **2012**, *52*, 284–294.

[6] G. Pascali, G. Mazzone, G. Saccomanni, C. Manera, P. A. Salvadori, *Nucl. Med. Biol.* **2010**, *37*, 547–555.

[7] G. Pascali, D. Panetta, S. Burchielli, M. De Simone, E. Sanguinetti, V. Lucchesi, S. Del Carlo, G. Saccomanni, C. Manera, M. Macchia, P. A. Salvadori, *J. Label. Compd. Radiopharm.* **2013**, *56*, P-213.

[8] G. Pascali, D. Panetta, S. Del Carlo, G. Saccomanni, C. Manera, M. Macchia, P. A. Salvadori, *J. Nucl. Med.* **2012**, *53*, 1632.

[9] G. Saccomanni, G. Pascali, S. Del Carlo, D. Panetta, M. De Simone, S. Bertini, S. Burchielli, M. Digiacomo, M. Macchia, C. Manera, P. A. Salvadori, *Bioorg. Med. Chem. Lett.* **2015**, *25*, 2532–2535.

[10] G. Pascali, L. Matesic, T. L. Collier, N. Wyatt, B. H. Fraser, T. Q. Pham, P. a Salvadori, I. Greguric, *Nat. Protoc.* **2014**, *9*, 2017–29.

[11] L. Matesic, I. Greguric, G. Pascali, *Aust. J. Chem.* **2018**, *71*, 811–817.

[12] L. Matesic, A. Kallinen, I. Greguric, G. Pascali, *Nucl. Med. Biol.* **2017**, *52*, 24–31.

[13] J. Ungersboeck, S. Richter, L. Collier, M. Mitterhauser, G. Karanikas, R. Lanzenberger, R. Dudczak, W. Wadsak, *Nucl. Med. Biol.* **2012**, *39*, 1087–1092.

[14] G. Pascali, A. Berton, M. DeSimone, N. Wyatt, L. Matesic, I. Greguric, P. A. Salvadori, *Appl. Radiat. Isot.* **2014**, *84*, 40–47.

[15] V. Arima, G. Pascali, O. Lade, H. R. Kretschmer, I. Bernsdorf, V. Hammond, P. Watts, F. De Leonardis, M. D. Tarn, N. Pamme, B. Z. Cvetkovic, P. S. Dittrich, N. Vasovic, R. Duane, A. Jaksic, A. Zacheo, A. Zizzari, L. Marra, E. Perrone, P. A. Salvadori, R. Rinaldi, *Lab Chip* **2013**, *13*, 2328–2336.

[16] J. Ungersboeck, C. Philippe, L.-K. Mien, D. Haeusler, K. Shanab, R. Lanzenberger, H. Spreitzer, B. K. Keppler, R. Dudczak, K. Kletter, M. Mitterhauser, W. Wadsak, *Nucl. Med. Biol.* **2011**, *38*, 427–34.

[17] K. E. Lewis, A. L. Rasmussen, W. Bennett, A. King, A. K. West, R. S. Chung, M. Chuah, *J. Neuroinflammation* **2014**, *11*, 55.

[18] J. Ashton, M. Glass, *Curr. Neuropharmacol.* **2007**, *5*, 73–80.

[19] E. A. Horne, N. Stella, *Future Lipidol.* **2008**, *3*, 435–452.

[20] M. Leitner, S. Menzies, C. Lutz, *Jax* **2009**, 1–28.

[21] R. Ahmad, M. Koole, N. Evens, K. Serdons, A. Verbruggen, G. Bormans, K. Van Laere, *Mol. Imaging Biol.* **2013**, *15*, 384–390.

[22] J. Logan, J. S. Fowler, N. D. Volkow, A. P. Wolf, S. L. Dewey, D. J. Schlyer, R. R. MacGregor, R. Hitzemann, B. Bendriem, S. John Gatley, D. R. Christman, *J. Cereb. Blood Flow Metab.* **1990**, *10*, 740–747.

[23] J. Logan, J. S. Fowler, N. D. Volkow, G. J. Wang, Y. S. Ding, D. L. Alexoff, *J. Cereb. Blood Flow Metab.* **1996**, *16*, 834–840.

[24] M. A. Mintun, M. E. Raichle, M. R. Kilbourn, G. F. Wooten, M. J. Welch, *Ann. Neurol.* **1984**, *15*, 217–227.

[25] B. M. Mazoyer, R. H. Huesman, T. F. Budinger, B. L. Knittel, *J. Comput. Assist. Tomogr.* **1986**, *10*, 645–653.

[26] "002300 - B6SJL-Tg(SOD1*G93A)<dl>1Gur/J," can be found under https://www.jax.org/strain/002300, **n.d.**

[27] D. Panetta, N. Belcari, A. Del Guerra, A. Bartolomei, P. A. Salvadori, *Phys. Medica* **2012**, *28*, 166–173.

[28] T. Liistro, L. Guiducci, S. Burchielli, D. Panetta, N. Belcari, S. Pardini, A. Del Guerra, P. A. Salvadori, P. Iozzo, *J. Cereb. Blood Flow Metab.* **2010**, *30*, 895–899.

[29] S. Moehrs, M. Defrise, N. Belcari, A. Del Guerra, A. Bartoli, S. Fabbri, G. Zanetti, *Phys. Med. Biol.* **2008**, *53*, 6925–6945.